Communication

Au#PbS Core#Shell Nanocrystals: Plasmonic Absorption Enhancement and Electrical Doping via Intra-particle Charge Transfer

Jong-Soo Lee, Elena V. Shevchenko, and Dmitri V. Talapin

J. Am. Chem. Soc., **2008**, 130 (30), 9673-9675 • DOI: 10.1021/ja802890f • Publication Date (Web): 03 July 2008

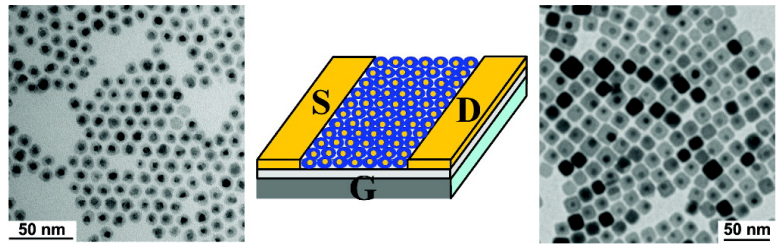

J|A|C|S
COMMUNICATIONS

Published on Web 07/03/2008

Au−PbS Core−Shell Nanocrystals: Plasmonic Absorption Enhancement and Electrical Doping via Intra-particle Charge Transfer

Jong-Soo Lee,[†,‡] Elena V. Shevchenko,[‡,§] and Dmitri V. Talapin*[,†,‡]

Department of Chemistry, University of Chicago, Chicago, Illinois 60637, The Molecular Foundry, Lawrence Berkeley National Laboratory, Berkeley, California 94720, and Center for Nanoscale Materials, Argonne National Laboratory, Argonne, Illinois 60439

Received April 24, 2008; E-mail: dvtalapin@uchicago.edu

Colloidal nanocrystals display size-dependent electronic structure and could be used as the building blocks for electronic and optoelectronic devices including solar cells, photodetectors, and field-effect transistors.[1] Self-assembled nanocrystal solids could combine superior electronic and optical properties of inorganic semiconductors with inexpensive solution-based low-temperature device fabrication important for solar cells and thermoelectric devices, for example. Arrays of close-packed PbSe and PbTe nanocrystals treated with hydrazine solution at room temperature can exhibit conductance of ~1 S cm^{-1} and carrier mobility above 1 cm^2/Vs.[1] Major fundamental problems that still need to be addressed are stable, controllable p- and n-type doping of nanocrystal solids.[2a] To date, several approaches such as charge transfer from species adsorbed at the nanocrystal surface[1,2b] and electrochemical doping[2c] have been explored. Recently, Urban et al. demonstrated that Ag_2Te nanoparticles can behave as p-dopants in their mixtures with PbTe nanocrystals.[2d]

Recent developments in colloidal chemistry allowed preparation of various multicomponent nanostructures such as core−shells, dumbbells, etc. with metal−metal,[3] metal−semiconductor,[4] and semiconductor−semiconductor[5] combinations. In this communication, we investigate the electronic properties of assemblies of heterostructured nanocrystals and propose a novel approach to doping of nanocrystal solids through the intraparticle charge transfer. Au−PbS core−shell nanostructures were chosen as a model system to study coupling effects between strongly confined metal and semiconductor phases. We compared optical and electronic properties of Au−PbS nanostructures with properties of their building blocks—Au and PbS nanocrystals (Figure 1a).[6] For a typical synthesis of Au−PbS core−shell nanostructures, 0.225 g of PbO, 5 mL of oleic acid, and 5 mL of 1-octadecene (ODE) were loaded in a 25 mL three-neck flask. The mixture was heated to 150 °C under vacuum to form Pb−oleate complex. After cooling the reaction mixture to 100 °C, dodecanethiol-capped Au nanocrystals (4.2 nm, 2 mg) dispersed in 1 mL of toluene[7] were added and toluene was distilled out. Growth of PbS shells was initiated by the injection of 0.13 mL of bis(trimethylsilyl)sulfide dissolved in 2 mL of ODE under vigorous stirring. The reaction mixture was kept at the injection temperature for 5−10 min and cooled to the room temperature followed by purification of nanocrystals from crude solution.[7] Au−PbS nanocrystals form stable colloidal solutions in chloroform, toluene, and tetrachloroethylene. PbS shell thickness can be controlled by the reaction time, concentration of Au seeds, and amount of injected sulfur precursor (Figure S1). The morphology of the PbS shell depends on the injection and growth temperatures. Uniform, nearly spherical PbS shells formed when the reaction was carried out at 100 °C (Figures 1b and S1). The shell was typically built of several crystal domains, as shown in Figure 1d.

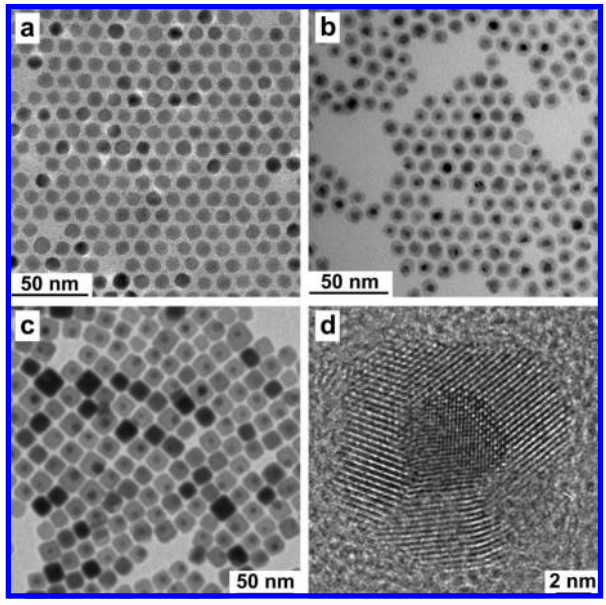

Figure 1. TEM images of (a) PbS nanocrystals and (b–d) Au−PbS nanostructures. (c) Cubic Au−PbS nanostructures synthesized at 150 °C. (d) Representative high-resolution TEM image of a Au−PbS core−shell nanostructure.

Increasing the growth temperature to 150 °C led to single-crystal cubic PbS particles grown from Au cores (Figure 1c). Narrow size distribution of as-synthesized Au−PbS nanostructures allowed their self-assembly into long-range ordered superlattices shown in Figure S2.

The X-ray diffraction patterns and analytical electron microscopy (EDX STEM) studies of Au−PbS nanostructures revealed the presence of fcc Au and rock-salt PbS phases (Figure 2a) and confirmed localization of Au atoms in the core and Pb, S atoms in the shell of Au−PbS nanostructures (Figure S3). Figure 2b shows the absorption spectra of Au cores and spherical Au−PbS core−shell nanostructures. The formation of the PbS shell around Au cores results in the shift of the surface plasmon resonance (SPR) absorption peak from 525 nm in bare Au to ~620 nm in Au−PbS core−shells (Figure 2b) due to the high dielectric constant of PbS.[8a,b] No pronounced SPR peak was observed in Au−PbS nanostructures with cores smaller than 2 nm (Figure S5). Au−PbS nanostructures do not show sharp excitonic features in near-IR. Instead, in monodisperse Au−PbS samples, we observed a broad near-IR absorption band (Figure 2b, inset). The broadening of

[†] University of Chicago.
[‡] Lawrence Berkeley National Laboratory.
[§] Argonne National Laboratory.

10.1021/ja802890f CCC: $40.75

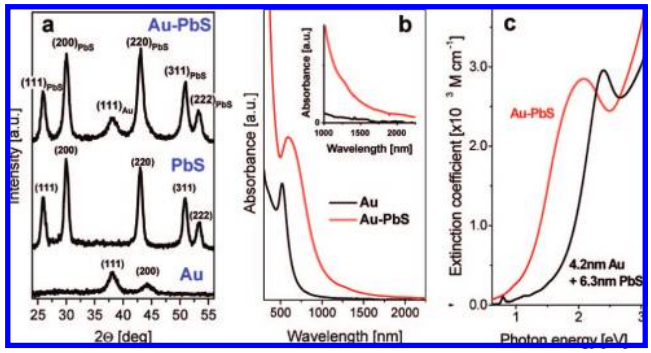

Figure 2. (a) Powder X-ray (Cu Kα radiation) diffraction patterns of Au, PbS, and Au−PbS nanocrystals. (b) Absorption spectra of 4.2 nm Au nanocrystals (black) and Au−PbS core−shell nanostructures with 2.6 nm thick PbS shells (red) dispersed in tetrachloroethylene. Inset shows magnified near-IR part of the spectra. (c) Extinction coefficient of Au−PbS core−shells with formal composition $Au_{0.55}(PbS)_{0.45}$ normalized to the molar concentration of $Au_{0.55}(PbS)_{0.45}$ "units" (red) and the extinction coefficients for noninteracting 4.2 nm Au and 6.3 nm PbS nanocrystals mixed with the same component ratio as in Au−PbS core−shells (black). See text for details.[7]

excitonic transitions was recently predicted for metal−semiconductor "molecules" due to coupling between excitons and plasmons.[9]

SPR at the Au surface generates a strong local optical field which persists into surrounding dielectric for about 10 nm.[10] This field enhancement can exist far from the resonant plasmon excitation energy.[10b] The core−shell morphology of Au−PbS particles provides ideal conditions for coupling transition dipole in the PbS shell to the plasmon field. To study possible synergistic coupling effects, we compared the extinction coefficients (ϵ) for Au−PbS core−shells with those for separated Au and PbS nanocrystals.[7] Figures 2c and S6 show ϵ values normalized to the molar concentration of hypothetic $Au_x(PbS)_{1-x}$ units and compared with the extinction of noninteracting Au and PbS nanocrystals calculated as $x\epsilon_{Au} + (1 - x)\epsilon_{PbS}$ where x was measured by elemental analysis of Au−PbS nanostructures. ϵ_{Au} and ϵ_{PbS} were normalized to the molar concentrations of Au and PbS units, respectively.[7] The coupling between the Au core and the PbS shell results in enhanced extinction throughout a broad spectral range. Thus, ϵ of Au−PbS nanocrystals integrated from 400 nm to 2.0 μm shows ∼28% extinction enhancement compared to noninteracting Au and PbS nanocrystals (Figure 2c). This additional extinction can be due to the increase of SPR absorption of the Au core and generation of additional oscillator strength in the PbS shell via direct plasmon-to-exciton coupling.

For comparative study of electrical properties of Au, PbS, and Au−PbS nanostructures, we fabricated close-packed films of these particles (nanocrystal solids) on Si wafers covered with a 110 nm thick layer of SiO_2 gate oxide with Ti/Au electrodes patterned by photolithography (Figure 3a).[7] All as-deposited nanocrystals show very poor conductivities (∼10^{-10} S cm^{-1}) which we attributed to weak electronic coupling between nanoparticles separated with bulky oleic acid capping ligands.[1a] Replacement of oleic acid with hydrazine molecules resulted in significant increase of conductance of nanocrystal solids.[1a] Thus, treatment of pristine PbS nanocrystal films with 1.0 M solution of N_2H_4 in acetonitrile for 48 h results in ∼9 orders of magnitude increase in film conductance. Hydrazine is known as a n-type surface charge transfer dopant for PbSe,[1a] PbTe,[11] and CdSe[12] nanocrystals. PbS nanocrystal field-effect transistors show stable n-type gate effect after hydrazine treatment. At low source−drain voltage (V_{DS}), the current between source and drain electrodes (I_D) increases linearly with V_{DS} (Figure 3b), and at high V_{DS}, the current saturates as the channel "pinches off" near

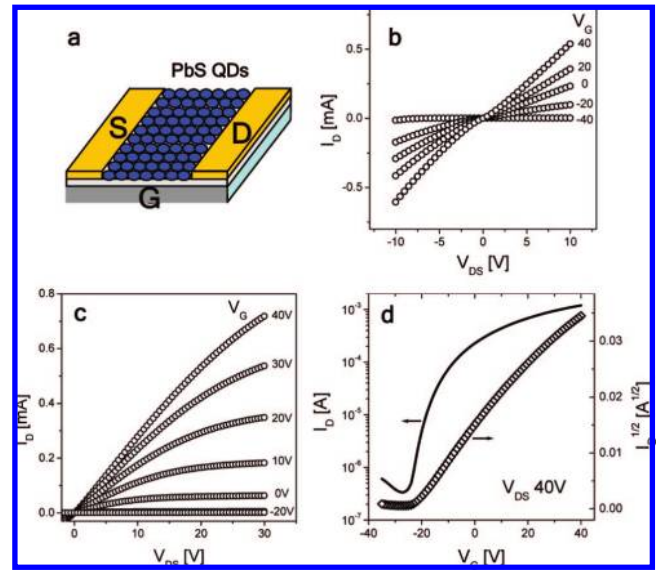

Figure 3. (a) Schematics of a field-effect transistor with channel comprising self-assembled PbS nanocrystals. (b) Plot of drain current I_D versus drain−source voltage V_{DS}, as a function of gate voltage V_G for a FET made of 7.1 nm PbS nanocrystals treated with 1 M solution of N_2H_4 in acetonitrile. The channel length L and width W were 4.5 ± 0.2 and 7500 μm, respectively. (c) I_D versus V_{DS} scans for different V_G for a nanocrystal FET made of 8.5 nm PbS nanocrystals treated with hydrazine solution for 48 h ($L = 10$ μm, $W = 2000$ μm). (d) Plots of I_D and $I_D^{1/2}$ versus V_G at constant $V_{DS} = 40$ V used to calculate current modulation and field-effect mobility in the saturation regime for n-channel FET assembled from 8.5 nm PbSe nanocrystals. $L = 10$ μm, $W = 2000$ μm.

the drain electrode (Figure 3c). Figure 3d shows current modulation $I_{on}/I_{off} > 10^3$ for an n-channel PbS nanocrystal FET with some hysteresis between the V_G scans in the forward and reverse directions (Figure S8). The hysteresis in I_D-V_G scans is common for devices using thick layers of gate oxide and typically associated with charge trapping in the gate oxide or semiconductor. The field-effect mobility of n-FET assembled from 8.5 nm PbS nanocrystals is $\mu_{lin} \sim 0.08$ cm^2 V^{-1} s^{-1} in the linear regime and $\mu_{sat} \sim 0.12$ cm^2 V^{-1} s^{-1} in the saturation regime.[7] PbS nanocrystal transistors show rather stable n-type operation. Presumably, hydrazine strongly absorbs at PbS surface, providing stable n-doping of nanocrystal solids. Films of dodecanethiol-capped Au nanocrystals show nonlinear $I-V$ characteristics and high resistance (Figure S10a). Treatment of Au nanocrystals with hydrazine increases the film conductance typically by 3−4 orders of magnitude compared to as-deposited Au nanocrystals,[7] due to reducing the interparticle separation and lowering the Coulomb charging energy. Typical for metals, applying voltage to the gate electrode does not result in any current modulation.

Arrays of Au−PbS core−shell particles are highly conductive after treatment with 1 M solution of hydrazine in acetonitrile. In contrast to Au and PbS nanocrystal devices, which show none and n-type gate effects, respectively, the Au−PbS core−shell nanostructures always exhibit p-type gate effect. The drain current of Au−PbS core−shell FETs increases as the gate voltage varies from 40 to −40 V, although the field-effect carrier mobility in Au−PbS nanocrystal solids could not be accurately calculated here due to relatively small current modulation (Figures 4a,d and S8). Such behavior is characteristic of high doping density and holes as the major carriers in Au−PbS nanocrystal solids. The doping of Au−PbS nanocrystal solids could be explained by intra-particle charge transfer. Comparison of the work function of Au (5.1 eV)[13a] and electron affinity of bulk PbS (4.5 eV)[13b] predicts the alignment

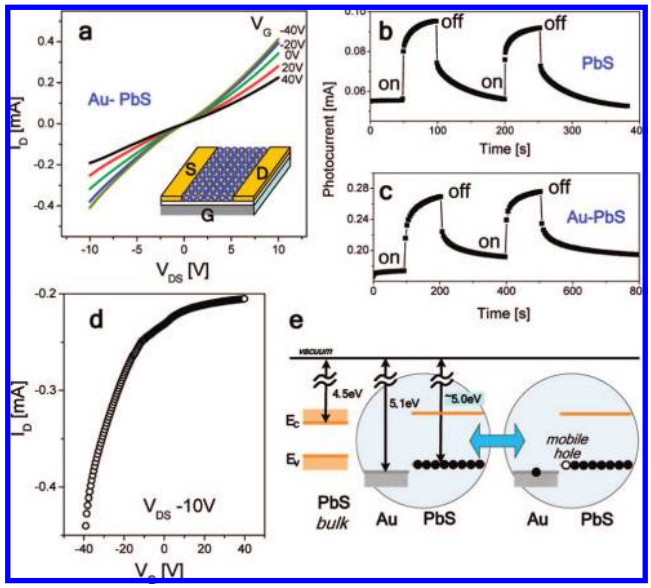

Figure 4. (a) $I-V$ scans for an array of 11 nm Au−PbS core−shell nanocrystals with 4.2 nm Au cores after exposure to 1 M solution of N_2H_4 in acetonitrile for 48 h. The channel length L and width W are 4.5 ± 0.2 and 7500 μm, respectively. Gate voltage V_G for each scan is shown in the graph. (b,c) Generation of photocurrent by (b) 8.5 nm PbS nanocrystals and (c) Au−PbS core shell nanocrystals under illumination with white light. (d) Plot of I_D versus V_G at constant $V_{DS} = -10$ V, showing p-type gate effect. $L = 4.5 \pm 0.2$ μm and $W = 7500$ μm. (e) Energy level diagram for Au−PbS core−shell nanocrystals predicts intraparticle charge transfer that creates mobile holes in PbS shell and leads to p-type doping of Au−PbS nanocrystal solids.

of energy levels in the Au core and the PbS shell favorable for charge transfer from the highest occupied $1S_h$ quantum confined state of the PbS shell to the Au core, as shown in Figure 4e. Very high static dielectric constant of the PbS shell (~175) facilitates such charge displacement, which can also be described as the injection of a mobile hole into the PbS shell. This effect is conceptually similar to charge transfer complex forming, for example, in tetrathiafulvalene−tetracyanoquinodimethane (TTF−TCNQ) system.[14] The exact amount of charge transferred between the Au core and the PbS shell and its dependence on the core size and shell thickness still have to be determined.

Above 200 K, the conductance of Au−PbS nanocrystal solids shows Arrhenius behavior with the activation energy of 45 meV (Figure S9). This behavior is characteristic of the transport dominated by the nearest-neighbor hops.[15] At lower temperatures, the activation energy sharply decreases to about 8 meV. Opposite to II−VI and III−V semiconductors, the band gap of PbS decreases with decreasing temperature.[16] This should lead to increased concentration of mobile holes in the Au−PbS nanocrystal solid at low temperature because of the larger energy difference between the states involved in the intraparticle charge transfer.

Both PbS and Au−PbS nanocrystal solids show similar efficiency of photocurrent generation under polychromatic illumination (Figure 4b,c). Efficient photocurrent generation shows that the presence of the Au core does not introduce fast channels for nonradiative recombination, which is rather surprising.[17] Further understanding of the photophysics of Au−PbS core−shell nanostructures will require detailed analysis of their electronic structure.

In summary, we synthesized multicomponent nanostructures with metallic Au core and semiconducting PbS shells. In Au−PbS core−shells, we observed enhancement of the absorption cross section due to synergistic coupling between plasmon and exciton in the core and shell, correspondingly. Field-effect devices with channels assembled from arrays of Au−PbS core−shell nanostructures demonstrate strong p-type doping that we attributed to the formation of an intra-particle charge transfer complex. We believe this work will provide the guidelines for designing solution-processed semiconductors with enhanced absorbance and controlled electronic doping for photovoltaic and thermoelectric applications. The core−shell morphology maximizes the interaction between the components and provides a convenient platform for studying exciton−plasmon interactions and other fundamental phenomena at the nanoscale. This approach can be applied to a variety of material combinations, such as metal−semiconductor, semiconductor−magnetic material, and so forth.

Acknowledgment. We thank A. P. Alivisatos (UC Berkeley), P. Guyot-Sionnest (University of Chicago) for stimulating discussions, and V. Altoe (LBNL) for help with analytical TEM studies. ICP-MS analysis was performed at ANL Analytical Laboratory. The work at the Molecular Foundry (LBNL) and Center for Nanoscale Materials (ANL) was supported by the U.S Department of Energy under Contract Nos. DE-AC02-05CH11231 and DE-AC02-05CH11357, correspondingly. D.V.T. acknowledges support from the University of Chicago and NSF MRSEC Program under Award Number DMR-0213745.

Supporting Information Available: Experimental details on synthesis and characterization, Supplementary figures as described in the text. This material is available free of charge via the Internet at http://pubs.acs.org.

References

(1) (a) Talapin, D. V.; Murray, C. B. *Science* **2005**, *310*, 86–89. (b) Konstantatos, G.; Howard, I.; Fischer, A.; Hoogland, S.; Clifford, J.; Klem, E.; Levina, L.; Sargent, E. H. *Nature* **2006**, *442*, 180–183.
(2) (a) Norris, D. J.; Efros, A. L.; Erwin, S. C. *Science* **2008**, *319*, 1776–1779. (b) Shim, M.; Guyot-Sionnest, P. *Nature* **2000**, *407*, 981. (c) Wang, C.; Shim, M.; Guyot-Sionnest, P. *Science* **2001**, *291*, 2390. (d) Urban, J. J.; Talapin, D. V.; Shevchenko, E. V.; Kagan, C. R.; Murray, C. B. *Nat. Mater.* **2007**, *6*, 115.
(3) Pellegrino, T.; Fiore, A.; Carlino, E.; Giannini, C.; Cozzoli, P. D.; Ciccarella, G.; Respaud, M.; Palmirotta, L.; Cingolani, R.; Manna, L. *J. Am. Chem. Soc.* **2006**, *128*, 6690.
(4) (a) Yang, J.; Elim, H. I.; Zhang, Q.; Lee, J. Y.; Ji, W. *J. Am. Chem. Soc.* **2006**, *128*, 11921–11926. (b) Mokari, T.; Aharoni, A.; Popov, I.; Banin, U. *Angew. Chem., Int. Ed.* **2006**, *45*, 8001–8005.
(5) (a) Talapin, D. V.; Mekis, I.; Gotzinger, S.; Kornowski, A; Benson, O.; Weller, H. *J. Phys. Chem. B* **2004**, *108*, 18826–18831. (b) Kim, S.; Fisher, B.; Eisler, H. J.; Bawendi, M. *J. Am. Chem. Soc.* **2003**, *125*, 11466–11467.
(6) Hines, M. A.; Scholes, G. D. *Adv. Mater.* **2003**, *15*, 1844.
(7) See Supporting Information for additional details.
(8) (a) Burda, C.; Chen, X.; Narayanan, R.; El-Sayed, M. A. *Chem. Rev.* **2005**, *105*, 1025–1102. (b) Shi, W.; Zeng, H.; Sahoo, Y.; Ohulchanskyy, T. Y.; Ding, Y.; Wang, Z. L.; Swihart, M.; Prasad, P. N. *Nano Lett.* **2006**, *6*, 875–881.
(9) Zhang, W.; Govorov, A. O.; Bryant, G. W. *Phys. Rev. Lett.* **2006**, *97*, 146804.
(10) (a) Zhang, J.; Chowdhury, M. H.; Lakowicz, J. R. *Nano Lett.* **2007**, *7*, 2101. (b) Rand, B. P.; Peumans, P.; Forrest, S. R. J. *Appl. Phys.* **2004**, *96*, 7519.
(11) Urban, J. J.; Talapin, D. V.; Shevchenko, E. V.; Murray, C. B. *J. Am. Chem. Soc.* **2006**, *128*, 3248.
(12) Lee, J.-S.; Talapin, D. V. Unpublished results.
(13) (a) Eastman, D. E. *Phys. Rev. B* **1970**, *2*, 1. (b) McDonald, S. A.; Cyr, P. W.; Levina, L.; Sargent, E. H. *Appl. Phys. Lett.* **2004**, *85*, 2089.
(14) Anderson, P. W.; Lee, P. A.; Saitoh, M. *Solid State Commun.* **1973**, *13*, 595.
(15) Mentzel, T. S.; Porter, V. J.; Geyer, S.; MacLean, K.; Bawendi, M. G.; Kastner, M. A. *Phys. Rev. B* **2008**, *77*, 075316.
(16) *Semiconductors:Physics of Nontetrahedrally Bonded Binary Compounds II*; Springer-Verlag; Berlin, 1983; Vol. III, p 17f.
(17) Liu, N.; Prall, B. S.; Klimov, V. I. *J. Am. Chem. Soc.* **2006**, *128*, 15362.

JA802890F